

● *Original Contribution*

MYOCARDIAL RAPID VELOCITY DISTRIBUTION

HIROSHI KANAI* and YOSHIRO KOIWA†

*Department of Electronic Engineering, Graduate School of Engineering; and †First Department of Internal Medicine, Graduate School of Medicine, Tohoku University, Sendai, Japan

(Received 9 June 2000; in final form 18 January 2001)

Abstract—Myocardial motion exhibits frequency components of up to 100 Hz, as found by a phased tracking method. To simultaneously measure the rapid and minute velocity signals at multiple points along the surface of the left ventricle (LV), in this study, conventional ultrasonic diagnosis equipment was modified to allow 10 scan lines from a sector scanner to be arbitrarily selected in real-time for analysis. By considering the maximum value of the velocity in the heart wall and the maximum depth from the chest surface, the number of transmission directions of the ultrasonic pulses should be carefully confirmed to be 10 to avoid aliasing, which is much less than the number employed in conventional tissue Doppler imaging (TDI). By applying the system, the velocity signals at about 240 points in the heart walls were simultaneously measured for three healthy volunteers. During a short period of 35 ms around end-diastole, the velocity signals varied spatially in the heart wall. At the end of systole, in the wavelets near the base of the interventricular septum (IVS), the slow pulse continued for about 30 ms, just before the radiation timing of the second heart sound. Then, a steep pulse occurred just at the timing of the closure of the aortic valve. The steep pulse at the base preceded that at the apex by several ms. By Fourier transforming each wavelet, the spatial distribution of the phase of the steep pulse components were clearly displayed. By applying the measurement method to two patients with aortic stenosis (AS), irregular vibration signals, which correspond to the murmur of the heart sound, could be directly detected during the ejection period. In conventional TDI, only the large slow movements due to the heartbeat are displayed, but these rapid and minute velocity components cannot be displayed. In this study, moreover, the phase components were detected for the first time from each of the velocity signals simultaneously measured at multiple points along the 10 scan lines. This measurement and method of analysis offer potential for new diagnostic techniques in cardiac dysfunction. (E-mail: hkanai@ecei.tohoku.ac.jp) © 2001 World Federation for Ultrasound in Medicine & Biology.

Key Words: Heart wall tracking, Heart wall vibration, Myocardial motion, Rapid and minute velocity, Spatial distribution, Left-ventricular end-diastolic pressure, Eigenvibration, Tissue Doppler imaging, Fourier analysis, *In vivo* experiments.

INTRODUCTION AND LITERATURE

Measurement of rapid motion in the heart wall has novel potential for use in diagnosis of regional myocardial motility and viability. In this paper, the measured “rapid motion” includes components with minute amplitude on the order of several tens of μm up to several hundred Hz, which has not been recognized in standard M-mode echocardiography, B-mode echocardiography, nor in TDI. It has already been experimentally shown that the Fourier spectra of the rapid motion up to 100 Hz has novel potential for use in diagnosis of myocardial fibrosis (Kanai et al. 1996) and that the frequency components

from 25 to 90 Hz contribute to regional myocardial thickening and thinning (Kanai et al. 1997). The rapid motion measured in this study should be distinguished from the slow motion displayed in the M-mode or B-mode images with large amplitude on the order of several hundred μm and with low frequency of less than 15 Hz.

Because tracking of the instantaneous position of the heart wall is indispensable in the above measurement, the correlation techniques previously devised for the measurement of blood flow (Dotti et al. 1976; Bassini et al. 1982; Bonnefous and Pesque 1986; Suorsa et al. 1990; Jensen 1991; Hein et al. 1993; Hein and O’Brien 1993) and small slow motion of tissue (Adler et al. 1990; Dickinson and Hill 1982; Tristram et al. 1988; de Jong et al. 1990; Hein et al. 1992) cannot be applied directly in the measurement.

Address correspondence to: Hiroshi Kanai, Department of Electronic Engineering, Graduate School of Engineering, Tohoku University, Sendai 980-8579, Japan. E-mail: hkanai@ecei.tohoku.ac.jp

The locations of the endocardium and epicardium are traced by analyzing the M-mode image (Fleming et al. 1994), but only large slow motion of the wall is followed. The specular reflectors in M-mode images are tracked from the cross-correlation along digitized M-mode lines (Adler et al. 1990). However, the spatial resolution is limited to several wavelengths, namely, those more than 1 mm.

In the estimation of two-dimensional (2-D) strain distribution or tissue elasticity (Ophir et al. 1991), the strain is estimated by correlation between the radiofrequency (RF) echo pair acquired at precompression and postcompression, but the minute strain that sequentially occurs during the compression process, is not considered.

In sonoelasticity imaging, using color Doppler instruments (Lerner et al. 1990; Parker et al. 1990) or the correlation technique (Yamakoshi et al. 1990; Catheline et al. 1999), 2-D spatial distribution of the amplitude and the phase of the actuated minute rapid motion in soft tissue or organs is displayed. The tracking operation, however, has not been applied.

In TDI, the previous 2-D color-flow mapping instruments have been modified to acquire low-frequency large-amplitude Doppler signals (Sutherland et al. 1994; Yamazaki et al. 1996). The translation velocity and rotation velocity in the LV short-axis view have been obtained (Watanabe et al. 1997) and the strain rate of the regional myocardium has been estimated (Heimdal et al. 1998). The velocity gradient, which assesses the regional myocardial contractility, is also shown (Fleming et al. 1994; Uematsu et al. 1995). Various reports have validated TDI clinically (Miyatake et al. 1995; Donovan et al. 1995). However, only large slow motion due to the heartbeat is displayed in TDI. At the same time, the velocity waveform in the heart wall is displayed at a low sampling frequency of about 30–40 Hz (Fleming et al. 1994; Yamazaki et al. 1996). The clinical meanings of the velocity waveform and the velocity gradients have been investigated (Palka et al. 1995, 1996; Goecsan et al. 1996). However, because the sampling frequency is not sufficiently high, the rapid and minute velocity components are not included in any of these results.

A digital echo-tracking method has also been applied to measure arterial wall motion, in which the zero-crossing point of the echo signal is tracked using a flip-flop-based device (Hokanson et al. 1970), the elaborate phase-locked loop technique (Hokanson et al. 1972; Sainz et al. 1976; Korba et al. 1979; Rapoport and Cousin 1982; Groves et al. 1982), or a high-speed A/D conversion system of 25 MHz (Hoeks et al. 1990). The spatial resolution in measurement of displacement is on the order of tens of mm. A digital wall-tracking system using counting clock pulses of 27 MHz has also been

proposed (Powalowski 1988). In these echo trackers, however, only the phase of the received RF signal is considered. Furthermore, it is easily affected by additive noise, as pointed out by Hartley et al. (1991), and it is difficult to lock onto and remain locked to the desired echo in *in vivo* experiments. As described in Kanai et al. (1996), to track the rapid and minute motion in the heart wall, the quantization error in the determination of the zero-crossing point or the rising edge is still large (several μm), even when the sampling clock frequency, f_{CLK} , is 100 MHz.

We have already developed a novel ultrasonic-based method, namely, the phased tracking method, to measure the rapid velocity in the heart wall by accurately tracking the movement $x_i(t)$ of a point (i) in the heart wall by the constraint least squares method applied to both the phase and magnitude of the quadrature-demodulated signals (Kanai et al. 1996). RF pulses are transmitted from an ultrasonic transducer at a pulse repetition interval ΔT , and the reflected ultrasonic wave is received by the same transducer and is multiplied by the original RF signal in quadrature demodulation. By synchronizing the pulse transmission timing and the acquisition timing in A/D conversion rigidly with the original RF signal, the achieved lower limit $|v_{\text{min}}|$ in the above velocity measurement is 0.1 mm/s, which was confirmed in phantom experiments (Kanai et al. 1997), using the developed method and system (Kanai et al. 1996). The lower limit depends on the small dispersion in the above synchronization and on the additive noise in the received signal. Because the lower limit $|v_{\text{min}}|$ is less than 1/2000 of the upper limit $|v_{\text{max}}|$ of the measurable velocity, which is free from aliasing, the dynamic range of the velocity measurement is given by $20 \log_{10} |v_{\text{max}}|/|v_{\text{min}}| = 73 \text{ dB}$. In phantom experiments (Kanai et al. 1996), a vibration with small amplitude of 20 μm generated on the large motion with an amplitude of $\pm 7.5 \text{ mm}$ and a frequency of 1 Hz, which simulates heartbeat, was successfully measured in the range from 1 Hz to 1 kHz.

Application of the quadrature demodulation shifts the spectrum peak from around the frequency (f_0) of RF US to around d.c. in the frequency domain. So long as the employed acquisition frequency (f_s) in the A/D conversion is higher than the bandwidth of the original spectrum around f_0 , no information is lost by the quadrature demodulation. For this measurement method, therefore, there are two kinds of spatial resolution along an ultrasonic beam; one is the minimum spatial interval between the succeeding points presettable in the heart wall, which is determined by the original frequency and bandwidth and is about 500 μm in the system. The other is the lowest measurable displacement or change in thickness between two points, which is dependent on precision in the above synchronization and additive noise

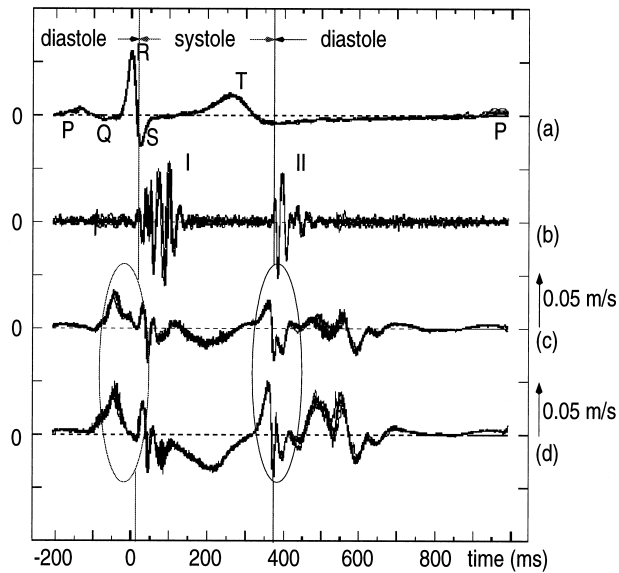


Fig. 1. Velocity signals on IVS measured by the phased tracking method for a healthy young subject. Five heartbeats are overlaid. The discriminative pulsive waves at end-diastole and end-systole are indicated by ovals.

and is about $0.5 \mu\text{m}$ in the system, confirmed in separate phantom experiments (Kanai et al. 1999c).

By applying this method and system to *in vivo* experiments, the velocity signal, $v(t; x_i)$, of point i at a depth of x_i in the heart wall with small amplitudes, which are less than several μm on the large motion resulting from a heartbeat, can be successfully detected with reproducibility as shown in Fig. 1c and d. By applying frequency analysis to the resultant velocity signal, $v(t; x_i)$, of the heart wall, the Fourier spectrum of $v(t; x_i)$ has been obtained for the first time with sufficient reproducibility in the frequency range up to 100 Hz (Kanai et al. 1996). The developed method has already been realized in a real-time measurement system (Kanai et al. 1999a). Moreover, from the difference of the resultant velocity signals $\{v(t; x_i)\}$ between point x_i and its succeeding point x_{i+1} preset along the ultrasonic beam, a minute change in thickness of several tens of μm has been detected with spatial resolution of $0.5 \mu\text{m}$ (Kanai et al. 1999c), as described above. In this method, however, measurement of the velocity signal and the change in thickness is limited to multiple points along one scan line of an ultrasonic beam passing through the object region.

To increase precision in the diagnosis, it is necessary to display the spatial distribution of these factors without decreasing the temporal resolution and spatial resolution along the depth axis. In this paper, by employing multiple 1-D configurations, each of which shows the axial component along the ultrasonic beam with fast acquisition intervals, the 2-D spatial distribution of the

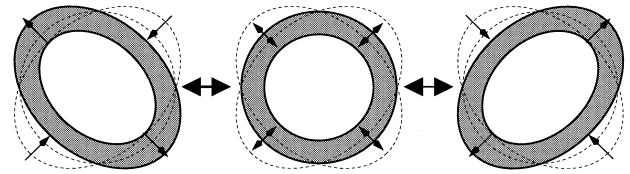


Fig. 2. Three phases of a mode-2 vibration of an elastic spherical shell.

rapid velocity components is obtained on the cross-sectional 2-D image.

The proposed method is applied to the following three fields in this paper.

1. Identification of mode-2 eigenvibration at end-diastole. LV pressure and its elasticity are significant parameters necessary for the clinical diagnosis of heart diseases. In particular, the LV end-diastolic pressure (LV-EDP), P_{ED} , is usually needed to assess the LV function in clinical settings. However, the LV-EDP, the normal value of which lies between 5 and 12 mmHg, cannot be obtained from the blood pressure measured at the brachial artery. Furthermore, the LV end-diastolic elasticity (LV-EDE), E_{ED} , cannot be noninvasively measured, and invasive catheterization is essential for the measurement of LV pressure of a patient. Though this measurement has high precision, such cardiac catheterization is difficult to apply at the bedside. Therefore, a noninvasive technique for measurement of LV-EDP (P_{ED}) and its elasticity, E_{ED} , is desired and has been developed as follows:

By approximating the LV wall vibration at end-diastole by a free vibration of an elastic shell, as shown in Fig. 2, Honda et al. (1994) have experimentally derived a simple relationship among the average Young's modulus E of the LV wall, LV internal radius r , LV wall thickness h , myocardial density ρ , and LV instantaneous eigenfrequency f_2 of the mode-2 eigenvibration. From experiments (Honda et al. 1994), it has been confirmed that the elasticity, E , of the shell is estimated from the two size parameters (r and h) and the mode-2 eigenfrequency f_2 without measuring LV-EDP.

By theoretical analysis (Mirsky et al. 1974), furthermore, the LV elastic stiffness, E_q , is given by the two size parameters (r and h) and the LV-EDP (P_{ED}). By assuming coincidence of the values of these two kinds of elasticity, E and E_q , which have been differently derived, the LV-EDP (P_{ED}) is determined from the eigenfrequency f_2 of the LV wall vibration and the two size parameters (r and h), which are measured by B-mode echocardiography.

In *in vivo* experiments, the vibration $v(t)$ on the LV side of the IVS is measured by the phased tracking method. By applying the short-time Fourier transform to $v(t)$, the instantaneous mode-2 eigenfrequency f_2 is determined at end-diastole. Using the f_2 , the LV-EDE (E_{ED}) and then the LV-EDP (P_{ED}) are determined. The procedure has already been applied to five patients (Kanai et al. 1999b). The estimates, $\widehat{E_{ED}}$, have a significant correlation with the ratio, P_{ED}/V_{ED} [mmHg/mL], which has been employed for evaluation of the cardiac function, where the LV-EDP (P_{ED}) is directly measured by catheterization and the LV end-diastolic volume V_{ED} is measured by angiocardiology. Furthermore, the resultant pressure estimate, $\widehat{P_{ED}}$, almost coincides with the actual one, P_{ED} , invasively measured by a catheter in the LV.

Though the mode-2 eigenvibration of the LV has been observed only in *in vitro* experiments with isolated canine hearts (Koiwa et al. 1988; Honda et al. 1994; Sato et al. 1996), it has not yet been confirmed in *in vivo* experiments with human hearts. Therefore, we applied the method developed in this study to the LV wall of four subjects to confirm that there is mode-2 vibration on the LV wall at end-diastole based on the spatial distribution of the frequency component around 30 Hz in the resultant vibrations $\{v(t; x_{kj})\}$. For this purpose, it is necessary to simultaneously measure the rapid velocity signals at points along each of multiple scan lines and to apply frequency analysis to each waveform.

2. Spatial delay-time detection of pulsive wave at end-systole. With the phased tracking method, it is possible to accurately detect small amplitude velocity signals of less than a few μm in the heart wall (Kanai et al. 1996). As shown in Fig. 1c and d, there are several remarkable pulsive waves during one cardiac cycle in the resultant velocity signals, two pulsive waves (slow positive pulse and succeeding steep negative pulse) being commonly obtained around end-systole for both healthy subjects and patients with myocardial fibrosis, but their powers were reduced in the patients (Kanai et al. 1996). These pulsive waves cannot be recognized in standard B-mode echocardiography, M-mode echocardiography, or in TDI. The physiological meanings and the mechanism of the pulsive waves have not been previously investigated at all. Herein, to consider the mechanism of these waves, the timing of the pulsive waves is simultaneously measured at the multiple points in the IVS and the LV posterior wall (LV-PW). For this purpose, it is necessary to detect the minute time-delay of several ms in the pulsive waves. If the mechanism of the pulsive waves

is clarified, it will offer potential for novel quantitative assessment of myocardial viability.

3. Irregular vibration during ejection period in AS. For patients with AS, a murmur, which is generated due to the irregular blood flow around the aortic valve, is generally detected during the ejection period in the heart sound. For such patients, on the other hand, if irregular vibrations are also directly detected in the heart wall by the phased tracking method, it will offer novel information regarding the origin of the murmur and the negative effect of the irregular blood flow on the myocardium.

For the above three applications, the following procedures are employed in this paper. From *in vivo* experiments, novel results were obtained.

METHOD

Principle of measurement of heart wall vibrations with tracking

RF pulses with an angular-frequency of $\omega_0 = 2\pi f_0$ are transmitted at a time interval of ΔT from an ultrasonic transducer on the chest surface. The ultrasonic pulse, reflected at an object with the depth x , is received by the same transducer. The phase difference $\Delta\theta(x; t)$ between the received signal $y(x; t)$ and the subsequently received signal $y(x; t + \Delta T)$ is given by:

$$\begin{aligned}\Delta\theta(x; t) &= \theta(x; t + \Delta T) - \theta(x; t) \\ &= \frac{2\omega_0}{c_0} \Delta x(t),\end{aligned}\quad (1)$$

where $\Delta x(t) = x(t + \Delta T) - x(t)$ is the movement of the object during the period ΔT from a time t and c_0 is the acoustic velocity in the human body. By dividing the movement Δx by the period ΔT , the average velocity $v(t + \Delta T/2)$ of the object during the period ΔT is given by:

$$\begin{aligned}\hat{v}\left(t + \frac{\Delta T}{2}\right) &= \frac{\Delta x(t)}{\Delta T} \\ &= \frac{c_0}{2\omega_0} \frac{\widehat{\Delta\theta}(x; t)}{\Delta T},\end{aligned}\quad (2)$$

where the phase difference $\widehat{\Delta\theta}(x; t)$ is accurately determined by the constraint least squares approach based on the complex cross-correlation between $y(x; t)$ and $y(x; t + \Delta T)$ for suppressing noise components, under the constraint that the signal waveform is invariant during ΔT but only the signal phase can change (Kanai et al. 1996). By multiplying the resultant velocity $\hat{v}(t +$

$\Delta T/2$) by the period ΔT , the next depth $\hat{x}(t + \Delta T)$ is estimated by:

$$\hat{x}(t + \Delta T) = \hat{x}(t) + \hat{v}\left(t + \frac{\Delta T}{2}\right) \times \Delta T. \quad (3)$$

By moving the depth of the object along the direction of the ultrasonic beam based on the resultant object depth $\hat{x}(t + \Delta T)$ by $\hat{v}(t + \Delta T/2) \times \Delta T$, the displacement of the object is successfully tracked, and then the velocity signal $\hat{v}(t + \Delta T/2)$ on the tracked large motion is accurately estimated (Kanai et al. 1996). This procedure is called the phased tracking method.

Limit in the number of scan lines from the ultrasonic probe

The time-domain complex cross-correlation technique is employed in this paper to maintain the spatial resolution, but it suffers from aliasing. In eqn (2), the phase difference during the pulse repetition interval, ΔT , must be less than π to avoid aliasing. Therefore, the upper limit in the velocity measurement, $|v_{\max}|$, is determined by:

$$|v_{\max}| < \frac{c_0 \pi}{2 \omega_0 \Delta T} = \frac{c_0}{4 f_0 \Delta T} = 0.77 \text{ m/s}. \quad (4)$$

In a typical case of $\Delta T = 167 \mu\text{s}$ and $f_0 = 3 \text{ MHz}$, the upper limit $|v_{\max}|$ is equal to 0.77 m/s.

To measure the velocity signals simultaneously at multiple points along the surface of the LV, the ultrasonic diagnostic equipment was modified so that N scan lines with directions $\{\theta_k\}$ ($k = 1, 2, \dots, N$) from a sector scanner are arbitrarily selected in real time using a microcomputer, as shown in Fig. 3, where $\{\cdot\}$ denotes set. In the employed phased-array ultrasonic probe, the direction of the ultrasonic beam in the fan-shaped region is identified by inputting the beam address, n_k , which is numbered from 0 to 239, into an 8-bit address register, which controls the direction θ_k of the k -th scan line from the phased-array ultrasonic probe. The number, N , of the directions should be increased as much as possible so as to increase the spatial resolution. For the heart wall, however, it is not easy to increase the number, N , of the transmission directions of the ultrasonic beams to definitely display the spatial distribution of the velocity on the cross-sectional image, as described below.

When N directions are selected from the above 240 addressable directions, the equivalent transmitted interval is lengthened to $N \times \Delta T$ from the repetition transmitted interval ΔT of the ultrasonic pulses, and the upper limit of the measurable velocity in eqn (4) is reduced to:

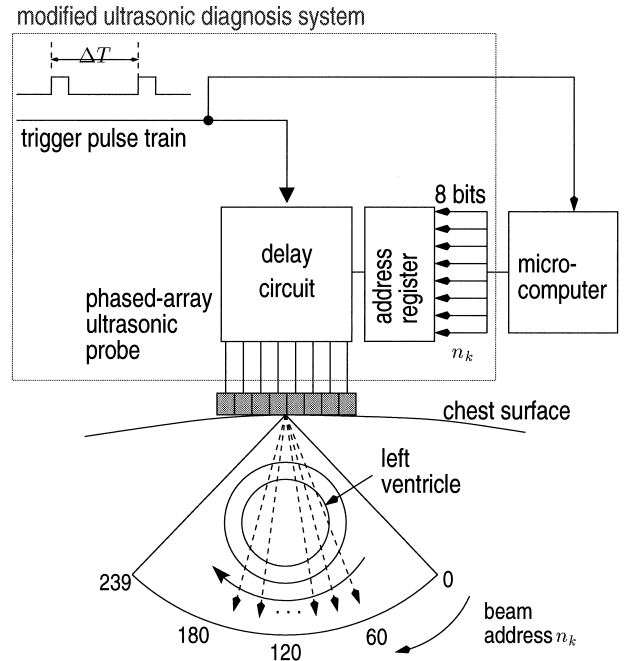


Fig. 3. A diagram illustrating simultaneous measurement of the velocity signals at multiple points on the LV wall by selecting 10 scan lines with directions $\{\theta_k\}$ from a sector scanner in real-time using a microcomputer.

$$|v_{\max, N}| = \frac{|v_{\max}|}{N} = \frac{c_0}{4 f_0 \Delta T N}. \quad (5)$$

The maximum value of the velocity at the points in the IVS or the LV-PW of the human heart is about 0.07 m/s (Kanai et al. 1996) in a typical case, which is about 1/10 of $|v_{\max}|$ in eqn (4). The maximum depth, d_{\max} , of the human LV-PW is about 120 mm from the chest surface. Therefore, the transmission interval ΔT of the ultrasonic pulses cannot be shorter than $2d_{\max}/c_0$ ($= 156 \mu\text{s}$). Thus, we must select 10 appropriate directions ($N = 10$) from the 240 directions addressable in the phased-array ultrasonic probe.

Let us consider the case where the number of the directions of the ultrasonic beams is equal to N at the measurement. If the addresses of the beams are assigned in the order of:

$$\underbrace{n_1, n_2, n_3, \dots, n_N}_{N\Delta T}, \underbrace{n_1, n_2, n_3, \dots, n_N}_{N\Delta T}, n_1, n_2, n_3, \dots, \quad (6)$$

the equivalent pulse repetition interval at each direction lengthens to $N \times \Delta T$. Therefore, the upper limit of eqn (4) becomes $|v_{\max}|/N$, as described in eqn (5).

Alternatively, for the procedure in which the transmission order of the beam is assigned as:

$$\begin{array}{c}
 n_1, n_1, n_2, n_2, n_3, n_3, \dots, n_{N-1}, n_{N-1}, n_N, n_N, n_1, n_1, n_2, n_2, \dots \\
 \leftarrow \Delta T \quad \leftarrow (2N-1)\Delta T \quad \leftarrow \Delta T \quad \leftarrow \dots \\
 \end{array} \quad (7)$$

the ultrasonic pulse is transmitted twice in every direction to determine the displacement of the object from the phase shift during ΔT . This procedure is employed in conventional color Doppler imaging and TDI. However, there are two kinds of equivalent pulse-repetition intervals, ΔT and $(2N - 1) \times \Delta T$. Thus, the measurable upper limit of the velocity is reduced to $|v_{\max}|/(2N - 1)$, which is about half of $|v_{\max,N}|$ in eqn (5). For the tracking operation in eqn (3), such error in the velocity estimated in the longer interval of $(2N - 1) \times \Delta T$ accumulates in one cardiac cycle and introduces serious errors. Therefore, we employ the transmission order of eqn (6) in *in vivo* measurements in the following sections.

Because the frequency components up to 100 Hz are significant in the novel diagnosis of the myocardium (Kanai et al. 1996, 1997) and the velocity signal on the heart wall is not stationary, the sampling frequency of the velocity signal should be higher than 200 Hz. By the transmission order of eqn (6), the equivalent sampling frequency is $1/(N \times \Delta T)$, as shown in Fig. 4a and about 600 Hz, which satisfies the above conditions when $\Delta T = 167 \mu\text{s}$ and $N = 10$. Note that, even by this procedure, a time lag of ΔT is caused in the sampling timing between the velocity wave $v_k(t)$ in the k -th direction and $v_{k+1}(t)$ in the $(k + 1)$ th direction and, for TDI, as shown in Fig. 4b, the time lag caused in the sampling timing between $v_k(t)$ and $v_{k+1}(t)$ is equal to $2M \times \Delta T$ and is much larger, where $M \times N$ is the number of the beam directions in the conventional TDI.

When all conditions are considered to be satisfied, the number, N , of the transmission direction of the ultrasonic pulses should be carefully confirmed to be 10, which is much less than the number employed in the conventional color Doppler method or TDI (*i.e.*, $M \times N$) which is more than 100.

RESULTS

By applying the phased tracking method described in the previous section to each j -th point preset along the k -th scan line of 10 directions, the velocity signals at about 12 points, $\{A_{k,j}\}$ ($k = 1, 2, \dots, 10$), from the RV

side to the LV side of the IVS and about 12 points, $\{B_{k,j}\}$ ($k = 1, 2, \dots, 10$), from the endocardium to the

epicardium in the LV-PW of a 21-year-old healthy male volunteer (subject N_A) were simultaneously measured. In the *in vivo* experiments, the employed pulse repetition interval ΔT and the ultrasonic frequency f_0 were $167 \mu\text{s}$ and 3 MHz, respectively. That is, the original pulse-repetition frequency ($\text{PRF} = 1/\Delta T$) was 6 kHz. The sampling frequency f_s in the A/D conversion of the quadrature demodulated US signal was 2 MHz.

Figure 5a shows the original cross-sectional B-mode image along the parasternal short-axis of the LV chamber at the timing of the R-wave of the electrocardiogram (ECG). The overlaid curved broken lines show the surfaces of the IVS, LV-PW, and the right ventricular (RV) wall. The ultrasonic beam was transmitted in 10 directions every 10th address from $n_1 = 80$ to $n_{10} = 170$. The 40 white dots in Fig. 5a show a portion of the measurement points on the RV side and LV side of the

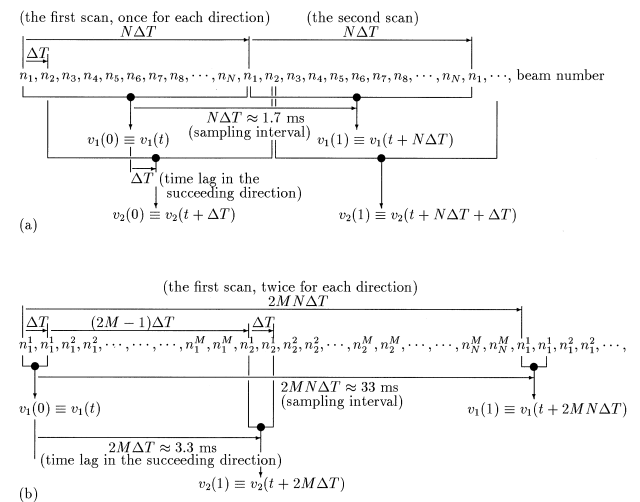


Fig. 4. The sampling timing and delay time between the digitalized velocity signals $v_k(n)$ in the k -th direction when the number, N , of beam directions in the proposed method is 10 and $\Delta T = 167 \mu\text{s}$. The product $M \times N$ shows the number of beam directions in conventional TDI and is assumed to be 100 in this paper ($M = 10$). (a) By the method proposed in this paper; (b) by the conventional TDI method.

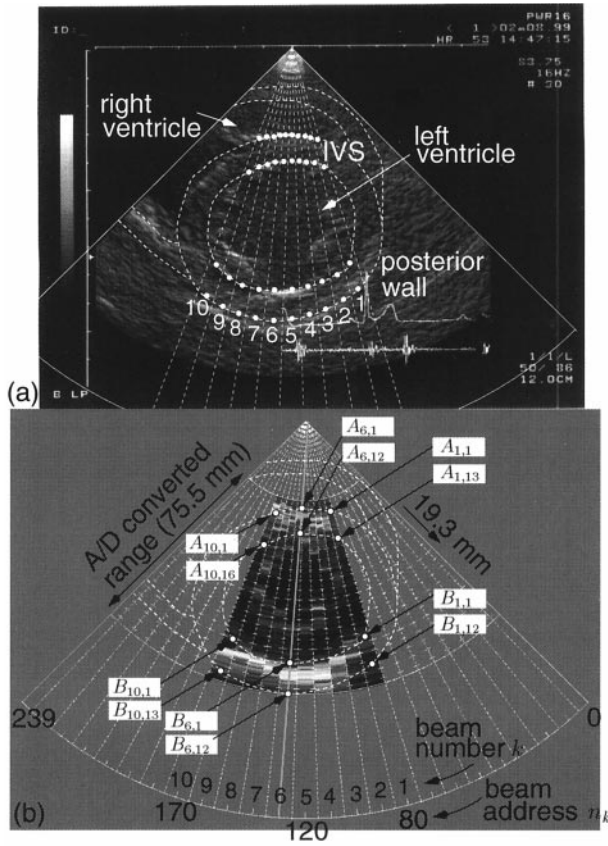


Fig. 5. (a) Original cross-sectional short-axis image of the LV of a 21-year-old healthy male volunteer (subject N_A) at the timing of the R-wave. The broken lines show the surface of the IVS and the LV-PW. Forty measurement points on the beams from the first to 10th address are also shown by white dots. (b) Reconstructed cross-sectional image of 10 directions of ultrasonic beams at the timing T_R of 6.7 ms after the R-wave.

IVS and the endocardial and epicardial sides of the LV-PW. Figure 5b shows the cross-sectional image reconstructed from the amplitude of the A/D converted data in each of 10 directions of ultrasonic beams at a timing of 6.7 ms after the R-wave. In this figure, the six dots from $A_{1,1}$ to $A_{10,16}$ and the six from $B_{1,1}$ to $B_{10,13}$ show the initial positions of the tracking points on the borders at the timing of end-diastole.

Figure 6 shows a typical example of the tracking results and the velocity signals at the four points in the sixth direction of the ultrasonic beam. Each depth of the four points, $A_{6,1}$ and $A_{6,12}$ on the RV and LV sides of the IVS and $B_{6,1}$ and $B_{6,12}$ on the endocardial and epicardial sides of the LV-PW, was manually preset at the timing of the R-wave. The tracking results $\{\hat{x}(t; A_{6,j})\}$ and $\{\hat{x}(t; B_{6,j})\}$ of these four points ($j = 1, 12$) are overlaid on the M-mode image, as shown in Fig. 6a. Their velocity signals, $\{\hat{v}(t; A_{6,j})\}$ and $\{\hat{v}(t; B_{6,j})\}$, at these four points are shown in Fig. 6d, e, f and g, respectively. The

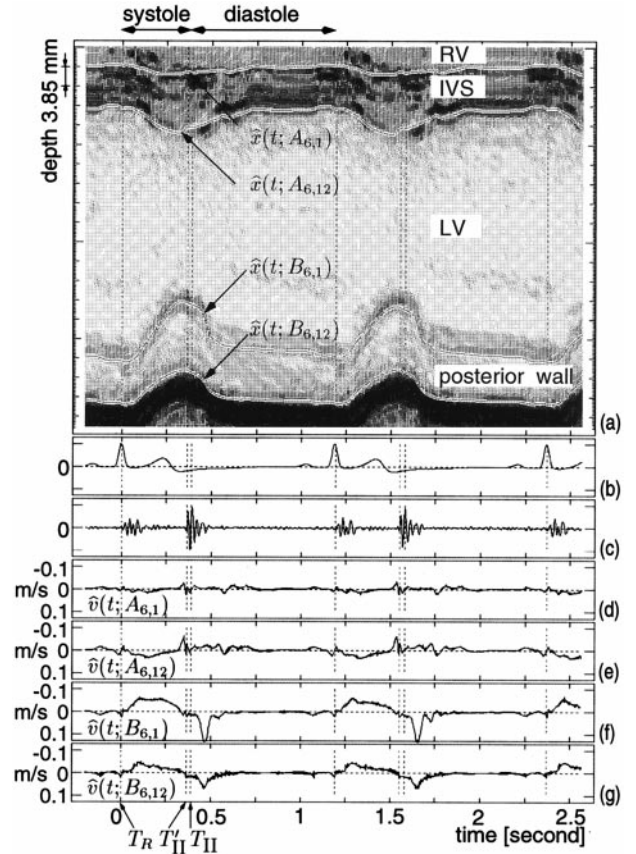


Fig. 6. *In vivo* experimental results of the LV vibrations at points $A_{6,1}$, $A_{6,12}$, $B_{6,1}$ and $B_{6,12}$ along the 6th ultrasonic beam for the same subject (subject N_A) as in Fig. 5. (a) Four tracking results $\hat{x}(t; A_{6,1})$ and $\hat{x}(t; A_{6,12})$ of the IVS, $\hat{x}(t; B_{6,1})$ and $\hat{x}(t; B_{6,12})$ of the LV-PW overlaid on the M-mode image, (b) ECG, (c) phonocardiogram (PCG), (d)(e) the velocity signals $\hat{v}(t; A_{6,1})$ and $\hat{v}(t; A_{6,12})$ of the IVS, (f)(g) the velocity signals $\hat{v}(t; B_{6,1})$ and $\hat{v}(t; B_{6,12})$ of the LV-PW; T_R -end-diastole and the display timing in Fig. 7; T'_{II} -the peak timing in the power of the second heart sound; T_{II} -the display timing in Fig. 11.)

resultant velocity signals were reproducible for two heartbeats. It has already been experimentally confirmed that these velocity components measured by the phased tracking method are reproducible in the frequency range from d.c. to 100 Hz (Kanai et al. 1996). Such rapid and small velocity components still cannot be observed by conventional ultrasonic equipment. During systole, the signals $\{\hat{v}(t; A_{k,j})\}$ and $\{\hat{v}(t; B_{k,j})\}$ have velocity components, so that the LV lumen contracts. At the beginning of diastole, on the contrary, they have velocity components so that the LV lumen expands.

The same tracking operation was applied to all of about 240 points $\{A_{k,j}, B_{k,j}\}$ ($k = 1, 2, \dots, 10, j = 1, 2, \dots$) preset at the timing of the R-wave at equal intervals of $385 \mu\text{m}$ ($= c_0/2f_s$) in the IVS and LV-PW along

each of the scan lines from n_1 to n_{10} . For each of about 240 points, the velocity signals $\{\hat{v}(t; A_{k,j})\}$ and $\{\hat{v}(t; B_{k,j})\}$ were obtained.

The direction of the scan line of n_6 in Fig. 5 was almost always perpendicular to the movement of both heart walls during one cardiac cycle, and the points $\{A_{6,j}\}$ and $\{B_{6,j}\}$ along the beam traced their movements. For the points along the beam other than n_6 , however, it was difficult to precisely trace the movement of the same region in the heart wall over time during one heartbeat because the direction of the ultrasonic beam was always fixed, but the heart chamber contracted during systole and expanded during diastole. Thus, the point, the depth of which was preset at the R-wave, slipped off the ultrasonic beam during systole. In a strict sense, therefore, each of the velocity signals $\{\hat{v}(t; A_{k,j})\}$ and $\{\hat{v}(t; B_{k,j})\}$ ($k \neq 6$) does not continuously reveal the accurate movement of each point for one cardiac cycle. However, for the short period of every several tens of ms, we can assume that these points stay at the same region in the heart wall. For example, during 30 ms, a region with an average speed of 0.03 m/s moves by 0.9 mm, which corresponds to the size of the focal area of the ultrasonic beam in the myocardium.

By the phased-tracking method we have developed, some discriminative pulsive waves have been found at end-systole, as shown in Fig. 1c and d, and their Fourier power spectra have potential for use in diagnosis of the heart (Kanai et al. 1996). At end-diastole, on the other hand, by applying the Fourier analysis to the signal, it has been experimentally found that a frequency component around 30 Hz is superior. In this study, therefore, the spatial distribution of these velocity signals was analyzed at end-diastole and end-systole, as described below.

For eigenvibration at end-diastole

Figure 7 shows a typical example of the wavelets of the simultaneously measured velocity signals $\{\hat{v}(t; A_{k,j})\}$ ($k = 1, 2, \dots, 10$) in the IVS and $\{\hat{v}(t; B_{k,j})\}$ in the LV-PW, respectively, at end-diastole. The central vertical axis in each wavelet shows a timing of T_R 6.7 ms after the R-wave in Fig. 6. Each amplitude of the velocity has already been manually corrected by dividing it by the cosine of the angle between the ultrasonic beam and the vector from the center of the LV at end-diastole to the measurement point in the heart wall. As shown in these wavelets, the waveforms gradually varied according to the directions of the ultrasonic beams at the timing of T_R . Along the left-hand side of Fig. 7, each point in the IVS and LV-PW moved upward towards the ultrasonic probe while, along the right-hand side of Fig. 7, each point had an opposite motion (*i.e.*, a downward velocity component).

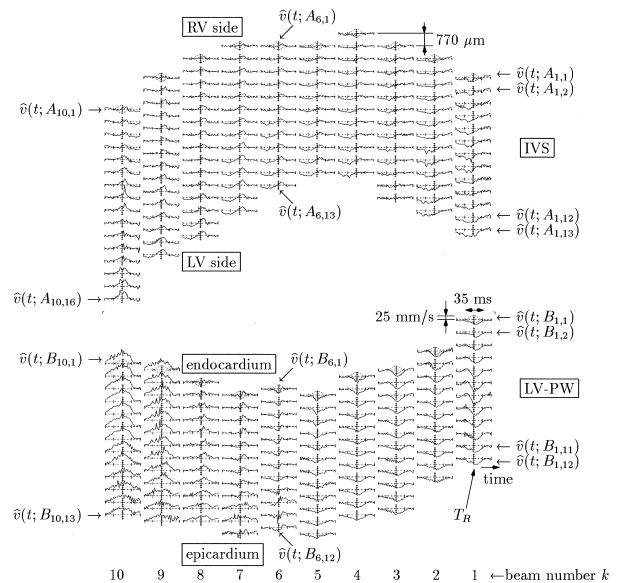


Fig. 7. The vibration velocity signals $\{\hat{v}(t; A_{k,j})\}$ and $\{\hat{v}(t; B_{k,j})\}$ ($k = 1, 2, \dots, 10$) at end-diastole of T_R in Fig. 6 (subject N_A) in the IVS (top) and LV-PW (bottom), respectively, along the scan lines in each of 10 directions.

Each instantaneous value of the velocity at the timing T_R is color-coded and the spatial distribution is displayed on the B-mode image in Fig. 8a. As shown in Fig. 4a, in a strict sense, a time lag of $(k-1)\Delta T = (k-1) \times 167 \mu\text{s}$ is hidden in the sampling timing of the velocity wave in the k -th direction of the scan lines ($k = 1, 2, \dots, 10$), where $\Delta T = 167 \mu\text{s}$. To simulate conventional TDI, on the other hand, Fig. 8b shows the color-coded instantaneous value of the velocity, but an extra time lag of $(k-1)2M\Delta T - (k-1)\Delta T = (k-1)(2M-1)\Delta T = (k-1) \times 2667 \mu\text{s}$ is added to the sampling timing of the points along the k th scan line from the points along the first scan line ($k = 1$), as shown in Fig. 4b, where $\Delta T = 167 \mu\text{s}$ and $M = 10$. There is a rapid change in the polarity of the velocity waveform, as shown in Fig. 8a, especially in the IVS. By conventional TDI, however, these instantaneous motions cannot be precisely displayed in Fig. 8b.

Moreover, to detect the spatial distribution of the phase of the eigenvibration components, the Fourier transform was applied to each wavelet of $\{\hat{v}(t; A_{k,j})\}$ and $\{\hat{v}(t; B_{k,j})\}$ in Fig. 7 after the Hanning window with a length of 35 ms was multiplied by each wavelet. The resultant instantaneous phase values at a frequency f_0 , $\{\phi(t; A_{k,j})\}$ and $\{\phi(t; B_{k,j})\}$ ($k = 1, 2, \dots, 10$) are color-coded and shown in Fig. 9a. The frequency f_0 was set at 23 Hz because the power spectrum has a peak at f_0 , which corresponds to the experimental values of the eigenfrequency of the human heart at end-diastole (Honda et al. 1998). In the phase values $\{\phi(t; B_{k,j})\}$ and

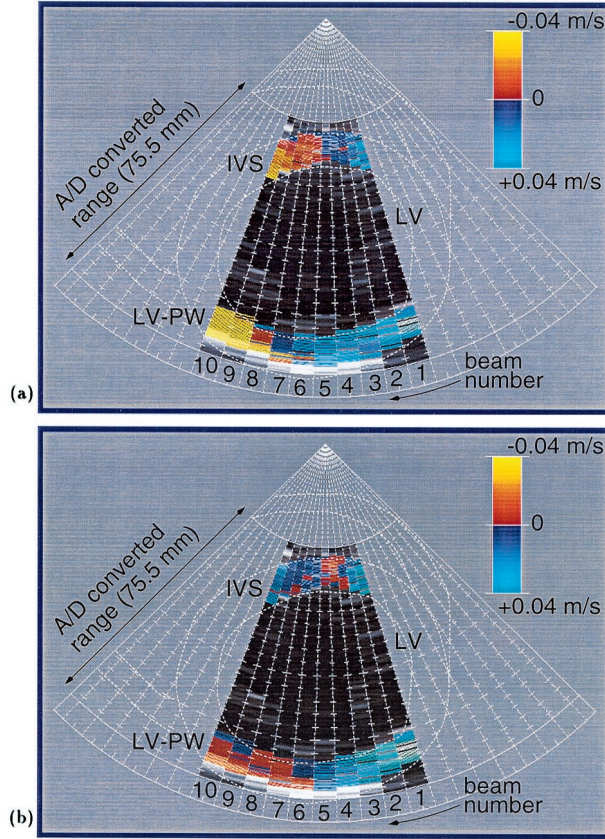


Fig. 8. Spatial distribution of color-coded velocity value of the measured wavelets at end-diastole (T_R in Fig. 6 of healthy subject N_A) on short-axis image corresponding to Fig. 7 (subject N_A). (a) By the method proposed in this paper; (b) by the conventional TDI method.

$\{\phi(t; B_{k,j})\}$, the time lag of $(k-1)\Delta T$ in measurements of $\{v(t, A_{k,j})\}$ and $\{v(t, B_{k,j})\}$ along the k -th scan line compared to measurements of $\{v(t, A_{1,j})\}$ and $\{v(t, B_{1,j})\}$ along the first scan line was corrected before the phase values were displayed.

As illustrated in the upper right of Fig. 9a, the value shows the phase delay of the measured wavelet when the cosine wave of 23 Hz is fitted. Both in the IVS and the LV-PW, the phase values vary from cyan (downward pulse) at the right-hand side, through blue and violet, to red (upward pulse) at the left-hand side. That is, the spatial distribution of the phase value at this timing does not conflict with the mode-2 eigenvibration of the LV chamber in the leftmost portion of Fig. 2.

For the cross-sectional view along the longitudinal-axis, on the other hand, similar processing was applied to the same subject N_A and the resultant spatial distribution of the phase values at end-diastole were overlaid on the longitudinal-axis cross-sectional image, as shown in Fig. 9b. The phase values along the eighth beam in Fig. 9b

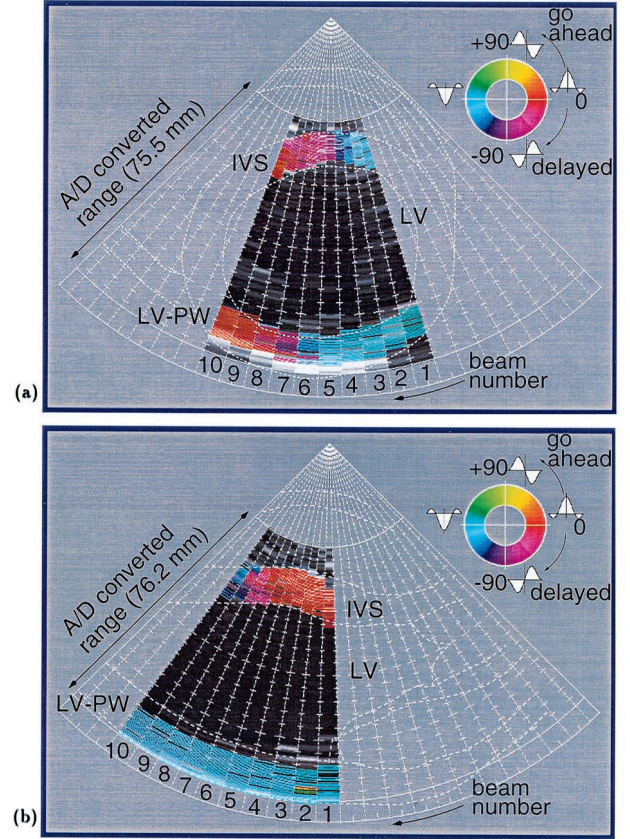


Fig. 9. Spatial distribution of color-coded phase value of the spectrum at 23 Hz of the measured wavelets at end-diastole (T_R in Fig. 6 of healthy subject N_A). (a) On short-axis image corresponding to Fig. 7; (b) on longitudinal-axis image.

were similar to those along the fifth beam in Fig. 9a. On the longitudinal-axis image in Fig. 9b, however, the phase value at the points in the IVS and LV-PW did not greatly vary from the base to near the apex; that is, each of these walls almost homogeneously moved on the longitudinal-axis plane, resulting in the expansion of the LV lumen at this timing of end-diastole.

By applying the same procedure in Fig. 9a to two other young healthy male subjects (N_B and N_C) and a patient with AS (subject P_A), the resultant spatial distributions of color-coded phase value of the spectrum of the measured wavelet at end-diastole are shown in Fig. 10, (1), (2) and (3), respectively. The employed frequency for N_B and N_C was the same as that for N_A in Fig. 9 but, for patient P_A , a lower frequency was employed. For both the IVS and LV-PW of subjects N_C in Fig. 10,(2) and P_A in Fig. 10,(3), the spatial distributions were similar to those for subject N_A in Fig. 9a; that is, the phase values vary from green or cyan (downward pulse) at the right-hand side, through yellow, to orange or red (upward pulse) at the left-hand side. For subject N_B in

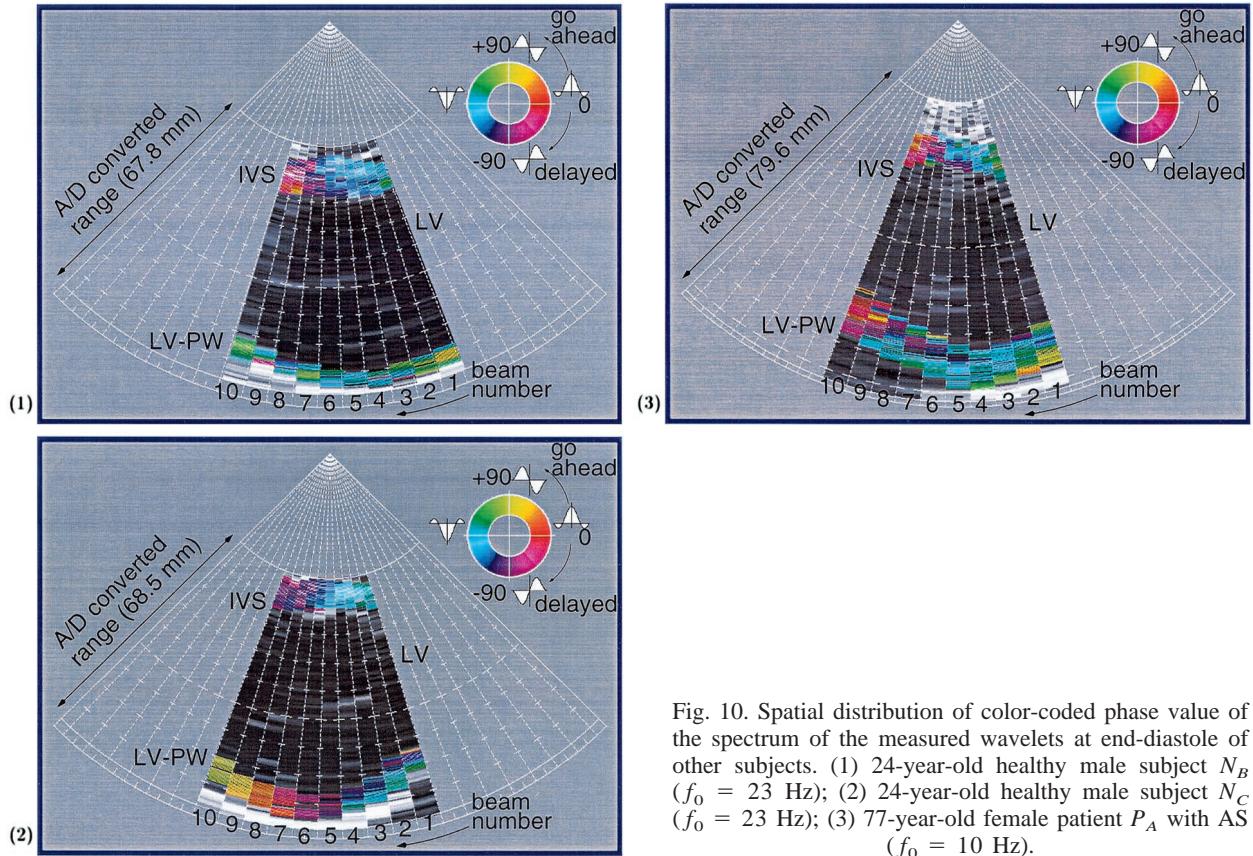


Fig. 10. Spatial distribution of color-coded phase value of the spectrum of the measured wavelets at end-diastole of other subjects. (1) 24-year-old healthy male subject N_B ($f_0 = 23$ Hz); (2) 24-year-old healthy male subject N_C ($f_0 = 23$ Hz); (3) 77-year-old female patient P_A with AS ($f_0 = 10$ Hz).

Fig. 10, (1), however, the change in phase from the right-hand side to the left-hand side was not clearly obtained for the LV-PW. For the IVS of N_B , however, spatial distributions similar to those of the other subjects were obtained.

For pulsive wave at end-systole

Figure 11 shows a typical example of the wavelets of the simultaneously measured velocity signals $\{\hat{v}(t; A_{k,j})\}$ ($k = 1, 2, \dots, 10$) in the IVS and $\{\hat{v}(t; B_{k,j})\}$ in the LV-PW at the timing T'_{II} of end-systole for healthy subject N_A in Fig. 6. The 10 scan lines were set on the longitudinal-axis cross-sectional image, as shown in Fig. 9b. The central vertical-axis in each wavelet shows the timing T'_{II} 25 ms before the peak timing T_{II} of the second heart sound. As shown in these wavelets near the base of the IVS, a slow upward pulse continued for about 30 ms before the timing T'_{II} ; that is, this slow pulse occurred before the closure of the aortic valve. Then, a steep downward pulsive wave occurred in the IVS around the timing T'_{II} at the beginning of the radiation timing of the second heart sound. The dip timing and the downward amplitude (dip depth) varied gradually from the base to the apex. That is, the downward steep pulse at the base preceded that at the apex and its amplitude gradually

decreased from the base to the apex. In the LV-PW, the gradual first pulse in the IVS was not clearly observed. A second steep pulsive wave was clearly obtained only at the points near the mitral valves or the left atrium (LA)

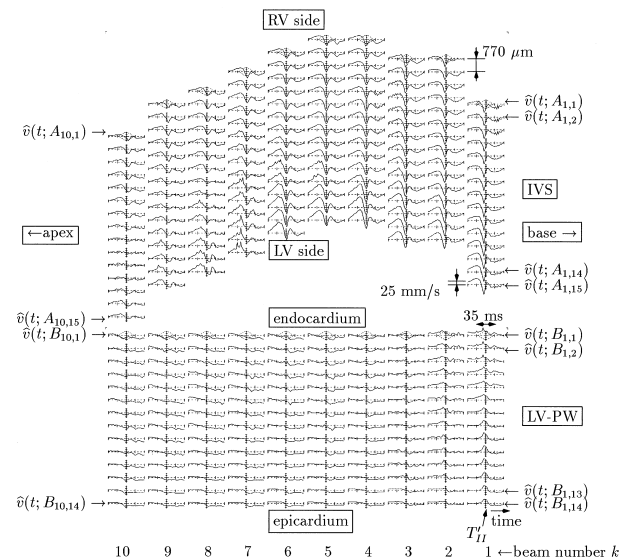


Fig. 11. Measured wavelets in IVS (top) and LV-PW (bottom) at end-systole (T'_{II} of Fig. 6 of subject N_A).

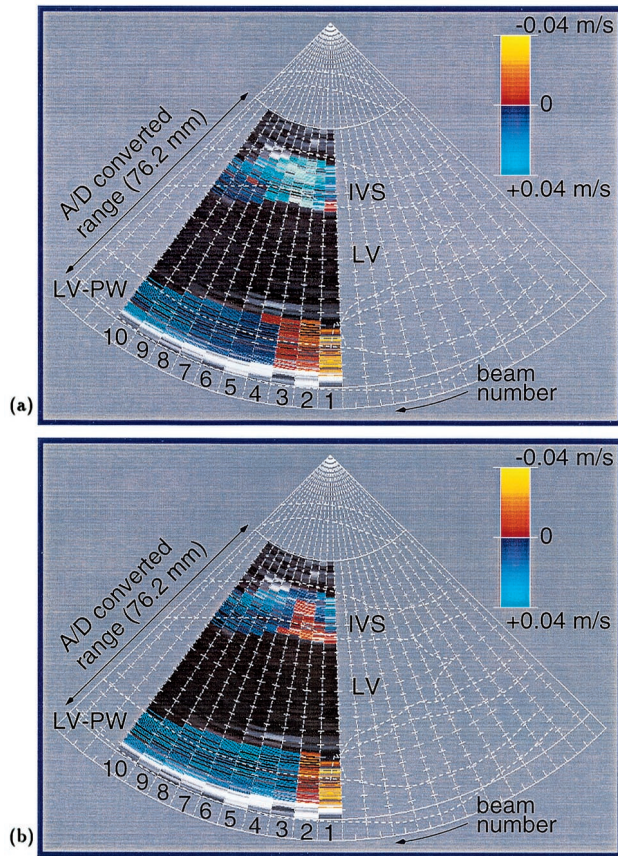


Fig. 12. Spatial distribution of color-coded instantaneous velocity value of the measured wavelets at end-systole (T'_{II} in Fig. 6 of subject N_A). (a) By the method proposed in this paper; (b) by the conventional TDI method.

along the right-hand side in Fig. 11, but the polarity was upward.

Similar to Fig. 8a and b, the spatial distribution of the instantaneous velocity component at the timing T'_{II} is shown in Fig. 12a and b, respectively. In Fig. 12b, a time lag was added to simulate the conventional TDI as in Fig. 8b.

To show the spatial distribution of the phase of the steep pulsive components, the Fourier transform was applied to each wavelet of $\{\hat{v}(t; A_{k,j})\}$ and $\{\hat{v}(t; B_{k,j})\}$ in Fig. 11 after the Hanning window with a length of 35 ms was multiplied by each wavelet. The resultant phase values at a frequency of 50 Hz are color-coded and shown in Fig. 13a, where the steep pulses have their peak power at around 50 Hz.

In the IVS represented in Fig. 13a, the phase values varied from violet (-100°) near the base, through cyan (-180°), to green (-220°) near the apex, as can be seen in Fig. 13b, which shows that the distribution of the time delay gradually increased from -4.4 ms near the base to $+2.2$ ms near the apex for the downward steep pulse

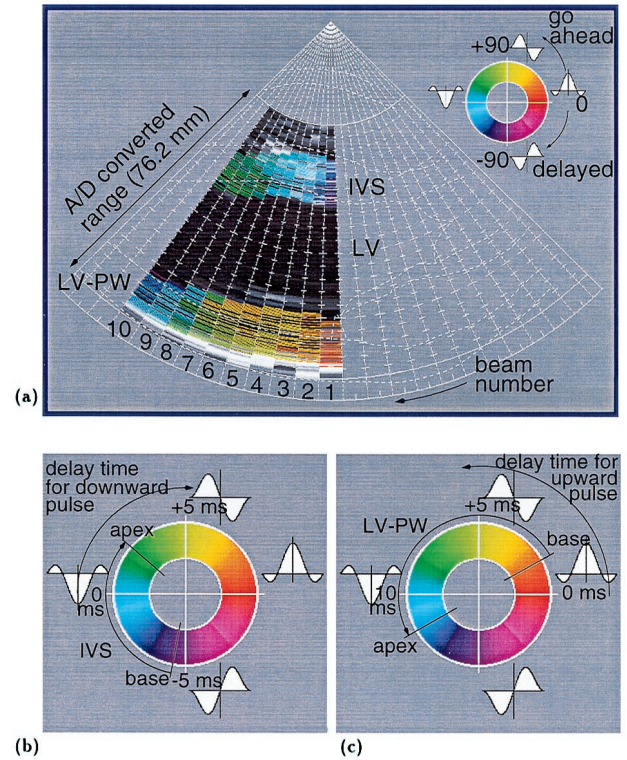


Fig. 13. (a) Spatial distribution of color-coded phase value of the spectrum at 50 Hz of the measured wavelets at end-systole on longitudinal-axis image corresponding to Fig. 11 of subject N_A . Illustrations showing (b) the delay time of the downward pulsive wave in the IVS and (c) the upward pulsive wave in the LV-PW.

around the timing T'_{II} in Fig. 11. In the LV-PW, on the other hand, the phase values varied from orange ($+30^\circ$) near the mitral valve, through yellow ($+90^\circ$) and green ($+150^\circ$) and, finally, to blue ($+210^\circ$) near the apex as shown in Fig. 13c, where it can be seen that the time delay of the upward pulse gradually increased from $+1.7$ ms near the base to $+11.7$ ms near the apex. Therefore, it is clearly evident that there is a delay of several ms from the base to the apex of the steep pulsive wave. However, such a time delay is not detected in either Fig. 12a or b because only the amplitude of the velocity waveform around the timing T'_{II} is considered.

By applying the same procedure in Fig. 13a to the two other healthy subjects, N_B and N_C in Fig. 10a and (2), and two patients with AS, subject P_A in Fig. 10,(3) and an 80-year-old male patient P_B , similar results were obtained for the IVS as shown in Fig. 14, (1), (2), (3) and (4), respectively. Though the frequency employed with both healthy subjects N_B and N_C was the same 50 Hz as that employed with subject N_A , for both patients P_A and P_B , the frequency employed was 10 Hz because noisy components that are generated by dis-

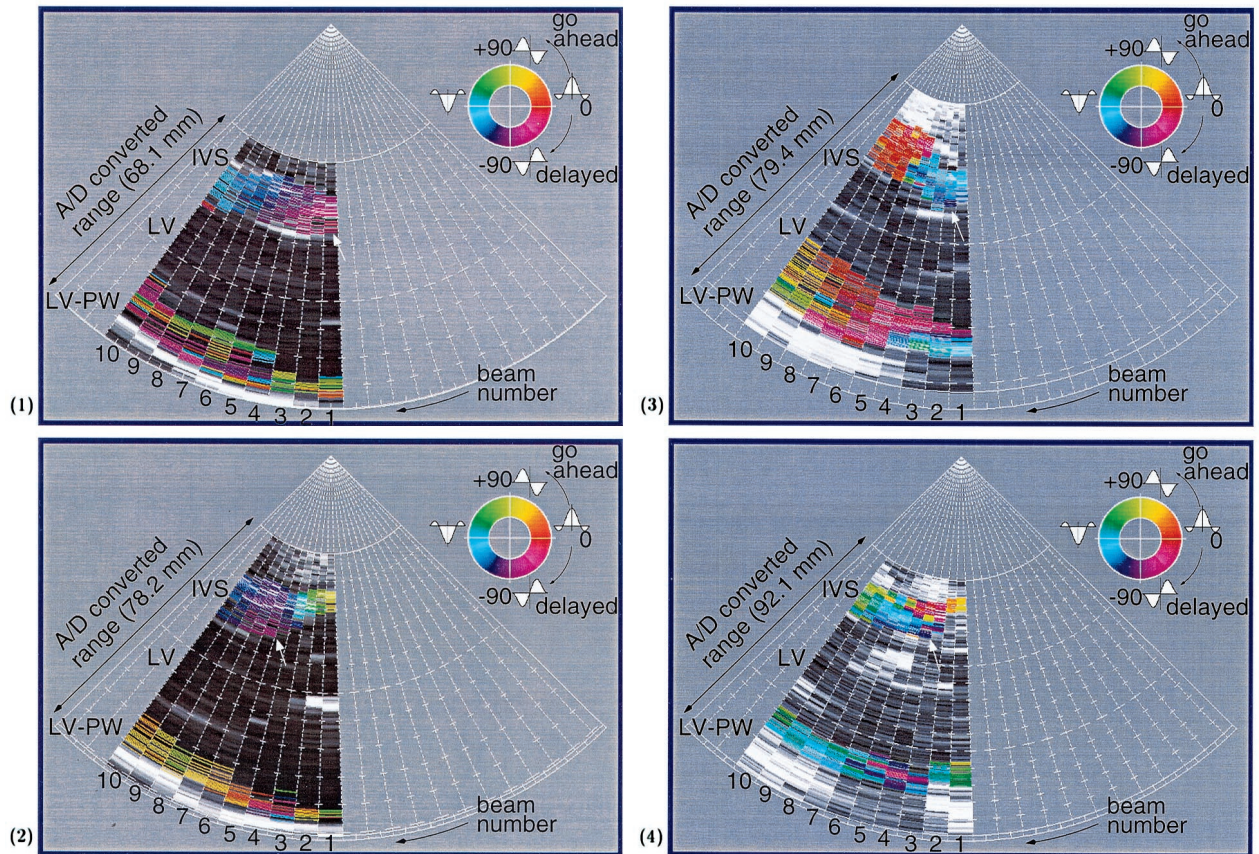


Fig. 14. Spatial distribution of color-coded phase value of the spectrum at 50 Hz of the measured wavelets at end-systole on longitudinal-axis image of the other four subjects. (1) 24-year-old healthy male subject N_B of Fig. 10a ($f_0 = 50$ Hz); (2) 24-year-old healthy male subject N_C of Fig. 10b ($f_0 = 50$ Hz); (3) 77-year-old female patient P_A with AS of Fig. 10c ($f_0 = 15$ Hz); (4) 80-year-old male patient P_B with AS ($f_0 = 15$ Hz).

ease were higher at 50 Hz. There is a clear time delay of several ms for the propagation of the negative pulse from the root of the aortic valve near the base to the apex side in the IVS. Especially for subjects N_B and N_C in Figs. 14, (1) and (2), from the root of the aortic valve (marked by white arrow), the pulsive wave propagates radially in the IVS. For the LV-PW, however, the pulsive signals were not clearly detected in these subjects other than N_A .

For irregular vibrations in the ejection period of patients with AS

The proposed method was applied to IVS and LV-PW along each of 10 scan lines set on the longitudinal axis cross-sectional image of patient P_A with AS. Acquired aortic valve stenosis often results from progressive degeneration and calcification of a congenitally defective bicuspid valve. Figure 15 shows the tracking results and velocity signals of the four points on both sides of IVS and LV-PW. AS leads to LV hypertrophy

and LV ischemia. The IVS became thickened to about 18 mm in patient P_A , as shown in the M-mode of Fig. 15a. Generally, one of the clinical features of AS is a systolic thrill at the base of the heart and a mid-systolic murmur, which was obtained in Fig. 15c, in the aortic area (Forbes and Jackson 1997). By the *in vivo* experiments in this study, moreover, noisy vibration signals, especially in the IVS in the ejection period, were observed for the first time, as shown in Figs. 15d and e. These noisy components are caused by the irregular blood flow in the stenotic aortic area.

Each of Figs. 16, 17 and 18 shows the waveforms of the simultaneously measured velocity signals $\{\hat{v}(t; A_{k,j})\}$ ($k = 1, 2, \dots, 10$) in the IVS and $\{\hat{v}(t; B_{k,j})\}$ in the LV-PW in the ejection period of healthy subject N_A , and of patients P_A and P_B , respectively. The center of the vertical axis in each waveform was determined by the mid-systolic timing of $T_{\text{sys}} = (T_R + T_{II})/2$, where T_R and T_{II} are the peak timing of the R-wave and the second heart sound, respectively, as shown in Fig. 15.

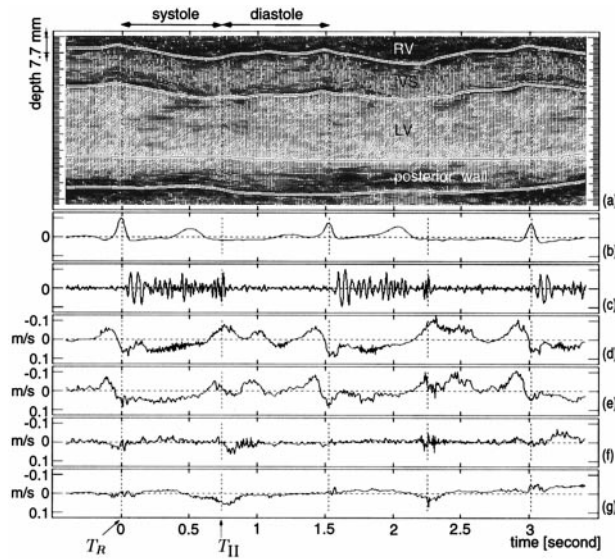


Fig. 15. *In vivo* experimental results of the LV vibrations at points $A_{8,1}$, $A_{8,24}$, $B_{8,1}$ and $B_{8,23}$ along the 8th ultrasonic beam for the same patient (P_A) with AS as in Figs. 10,(3) and 14,(4). (a) M-mode image and four tracking results $\hat{x}(t; A_{8,1})$ and $\hat{x}(t; A_{8,24})$ of the IVS, $\hat{x}(t; B_{8,1})$ and $\hat{x}(t; B_{8,23})$ of the LV-PW overlaid from top to bottom; (b) ECG; (c) phonocardiogram (PCG); (d)(e) the velocity signals $\hat{v}(t; A_{8,1})$ and $\hat{v}(t; A_{8,24})$ of the IVS; (f)(g) the velocity signals $\hat{v}(t; B_{8,1})$ and $\hat{v}(t; B_{8,23})$ of the LV-PW.

For healthy subject N_A of Fig. 16, at the points near the LV lumen of IVS and LV-PW, there were high-frequency components in the velocity signals during the ejection period. These components are due to the rapid blood flow during the ejection period. For patient P_A of Fig. 17, high-frequency components were observed at the points near the LV-PW endocardium, but at points almost in the IVS. For patient P_B of Fig. 18, especially near the root of the aortic valve of the base in the IVS, there were large noise components with high-frequency components around 100 Hz.

To quantitatively evaluate the power difference between the observed positions, 16 points were selected on the four layers of the RV side of IVS, the LV side of IVS, the LV-PW endocardium, and the LV-PW epicardium along the beams from the fourth to seventh scans, as enclosed by rectangles in Figs. 16, 17 and 18. By applying the Fourier transform to each signal at these 16 points in each of Figs. 16, 17 and 18, after multiplication by the Hanning window with a length of two or three hundreds ms, the power spectrum was obtained. The employed Hanning window is shown at the top of each column in these figures. By averaging the resultant power spectra at the points in each of the four layers, the results are shown in Fig. 19 (1), (3) and (4), respectively. By applying the

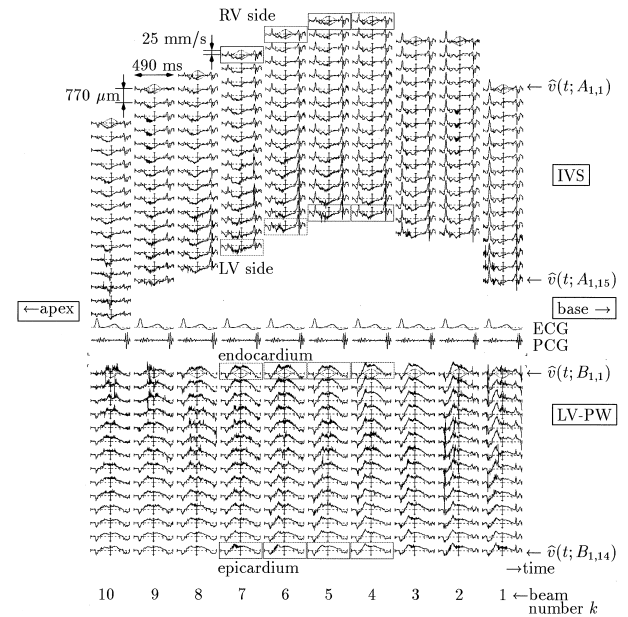


Fig. 16. Measured velocity signals along longitudinal-axis in IVS (top) and LV-PW (bottom) in ejection period of the same healthy subject (N_A) as in Figs. 5–9 and 11–13. The signals enclosed by rectangles in four layers are employed in Fig. 19a for evaluation of the averaged power spectra.

same procedure to healthy subject N_B , the result is shown in Fig. 19, (2).

For healthy subjects (N_A and N_B) in Fig. 19, (1) and (2), the low-frequency components around d.c. were large for both walls (IVS and LV-PW). At the same time, there were large power differences between the two layers in both walls, which shows that the change in thickness generated in each wall during the ejection period was large; for the IVS of P_A in Fig. 19, (3), however, the power was large. However, the power and power difference were not so large for the LV-PW of P_A in Fig. 19 (3) nor for either wall of P_B in Fig. 19 (4).

With regard to the high-frequency components in the signals of Fig. 17, for healthy subject N_A in Fig. 19 (1), the power spectrum at the point near the LV lumen of IVS and LV-PW had larger power in the frequency ranges from about 100 Hz to 120 Hz and from about 140 Hz to 180 Hz. The power spectra at the RV side of IVS and at the LV-PW epicardium were roughly similar. Similar results were obtained for subject N_B in Fig. 19 (2). Although for patient P_A in Fig. 19 (3), the RV side of IVS had a power spectrum similar to that of the LV side of IVS and the LV-PW endocardium. For patient P_B in Fig. 19 (4), the LV side of the IVS had a much larger power than the RV side of IVS. For both patients with AS, the power of the velocity signals in IVS was at least 5 dB larger than that in both healthy subjects N_A and N_B in the frequency range from 30 Hz to 200 Hz.

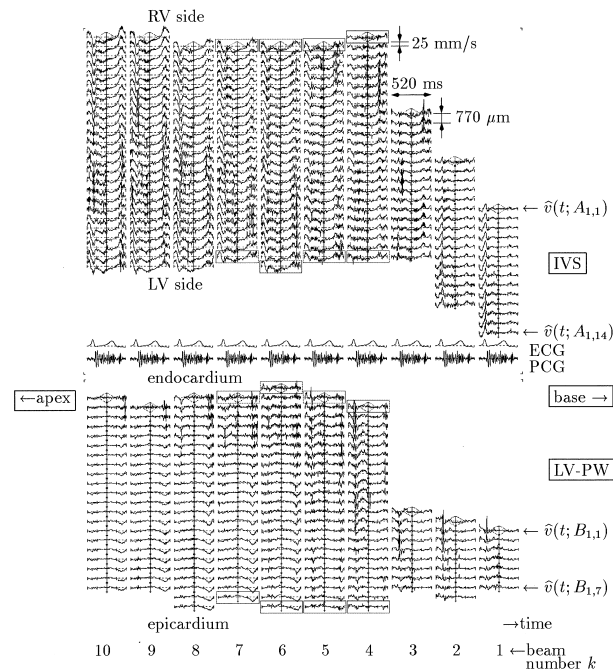


Fig. 17. Measured velocity signals along longitudinal-axis in IVS (top) and LV-PW (bottom) in ejection period of the same female patient (P_A) with AS as in Figs. 10,(3), 14,(3), and 15.

DISCUSSION

In this study, for each of about 20 points preset in the IVS and LV-PW along each of 10 scan lines, the velocity waveform was measured continuously for a few heartbeats. By applying the Fourier transform to the velocity wave, the power spectrum was obtained up to 100 Hz and the phase value at the frequency with the peak power was color-coded and displayed. The power of the high-velocity components up to several tens of Hz was less than 1/30 in amplitude of that of the large slow motion up to 10 Hz due to heartbeat. The wide dynamic range in amplitude up to 100 Hz was achieved in the measurement (Kanai et al. 1996).

When the instantaneous velocity is color-coded and displayed as a 2-D image, as shown in Figs. 8a and 12a, the results highly depend on the timing of the sampling. In the phase value at the peak frequency, however, the phase values were averaged during the period of the window length (35 ms) employed in the Fourier transform. Thus, the results did not highly depend on the timing. Moreover, the time lag in the scanning of the beam was corrected in Figs. 9 and 13a.

The large slow motion, on the order of several hundred μm up to 10 Hz, is displayed by conventional TDI. However, the displacement of each point is not tracked. For rapid small motion, on the order of several tens of μm up to 100 Hz, conventional TDI cannot

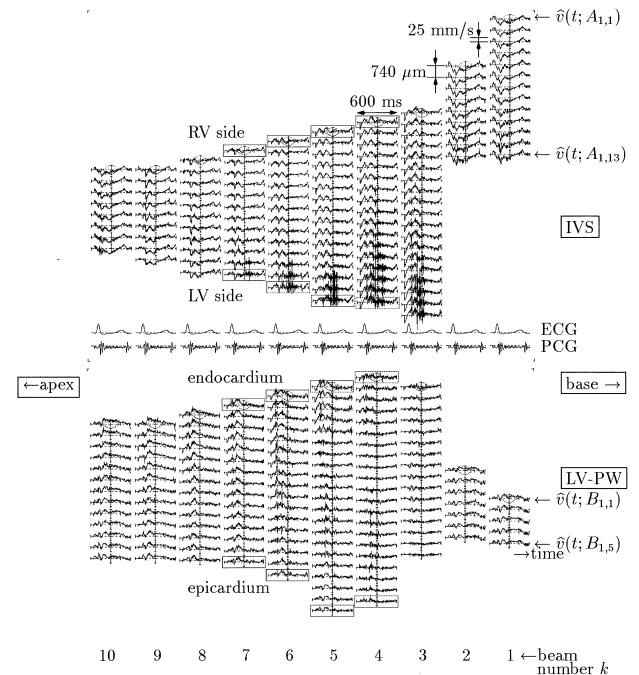


Fig. 18. Measured velocity signals along longitudinal-axis in IVS (top) and LV-PW (bottom) in ejection period of the same male patient (P_B) with AS as in Fig. 14,(4).

display it because the sampling frequency is about 30 Hz. In this study, the motion was tracked and accurately measured at a sampling frequency of 600 Hz, and its spatial distribution was displayed by restricting the number of the beam directions to 10 so as to avoid aliasing.

From the *in vivo* experiments, various results were obtained. For end-diastole, the phase values of the points along the fifth beam in the short-axis image in Fig. 9a were similar to those along the eighth beam in the longitudinal axis image in Fig. 9b. From these results from separate experiments, the promise of the measurements was confirmed.

The distribution of the phase value at 23 Hz in Fig. 9a and the instantaneous velocity values in Fig. 8a show that there was a mode-2 eigenvibration in the short-axis image, which has not been observed in conventional TDI methods. The reasons why such eigenvibration was excited, for example, by the blood flow at atrial systole, should be considered in the future.

For end-systole, on the other hand, the spatial distribution of the phase values of the pulsive wave which we found in the previous study (Kanai et al. 1996) at end-systole was definitely displayed for the first time in Fig. 13. The mechanism of the pulsive wave generated at end-systole should also be investigated in the future by *in vitro* and *in vivo* experiments. There are two possibilities: the propagation of the pulsive wave caused by the clo-

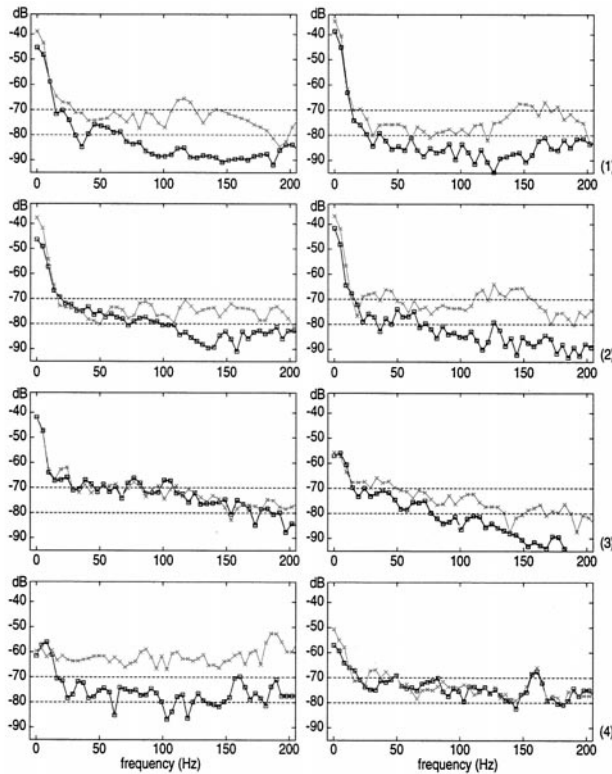


Fig. 19. Power spectra of measured velocity signals in ejection period averaged in the points from the fourth scan line to seventh scan line in each of four layers. left-hand side: for the RV-side of IVS (squares) and LV-side of IVS (crosses); right-hand side: for LV-PW endocardium-side (crosses) and LV-PW epicardium-side (squares). (1) For healthy subject N_A in Fig. 16; (2) For healthy subject N_B in Fig. 14,(1); (3) For patient P_A with AS in Fig. 17; (4) For patient P_B with AS in Fig. 18.

sure of the aortic valve and the time difference in the depolarization in each regional myocardium. For the former case, the propagation speed of the 50 Hz component was about 5 m/s in both IVS and LV-PW for healthy subject N_A in Fig. 13a because the distance from the base-side to the apex-side is 34 mm in IVS and 50 mm in LV-PW, and the delay is 6.6 ms in IVS and 10 ms in LV-PW. For the other healthy subjects, N_B and N_C in Fig. 14, (1) and (2), the propagation speed was also about 5–6 m/s. For patients P_A and P_B in 14, (3) and (4), however, the propagation speed of 10 Hz component was about one-tenth of the above value.

For patients with AS, it is well known that a murmur is radiated especially at systole (Constant 1985). However, the original vibration of the heart sound cannot be directly detected from the chest surface using a stethoscope or a microphone. In this study, the myocardial vibration that corresponds to the murmur was directly detected for the first time. The spatial distribution of the myocardial irregular vibration should be investigated in

more detail by increasing the number of patients. Moreover, the effects of the irregular vibration on the heart function and the myocardium should be clarified in the future because it is already known that the actuated vibration on the order of several tens of Hz in systole rapidly affects the contraction of the myocardium (Janssen et al. 1996; Koiwa et al. 1997).

Further possible applications of the technique proposed in this paper are as follows:

1. The different transmural layers of the myocardium have transmural heterogeneity with respect to the microvascular flow, metabolic consumption and the strength of contraction. The method developed in this study can reveal the intramyocardial contraction/relaxation heterogeneity by evaluating the change in thickness or its speed in two dimensions.
2. By *in vivo* experiments represented in Figs. 8a and 9a, the mode-2 vibration was confirmed. Thus, using this mode, the end-diastolic pressure and the average elastic property of the heart wall can be obtained, as described in the Introduction.
3. A discriminative pulsive wave at end-systole was found in the measured velocity waveform in our previous study (Kanai et al. 1996). The power spectra of patients with fibrosis were different from those of healthy subjects. The origin and the mechanism of the pulsive wave should be investigated continuously, based on the method developed in this paper for the development of a novel method of diagnosis.

The following problems remain to be solved:

1. In the velocity measurement employed, based on the cross-correlation between the quadrature-demodulated signals of the succeeding received signals, spatial averaging of the phase shifts due to the displacement around each measurement point is unavoidable. As described in the Introduction, the minimum interval between the succeeding points presettable in the heart wall is determined by the original frequency and bandwidth and is about 500 μm in the system. In this paper, we have assumed that the velocity is spatially constant in the region, with a width of 500 μm around each measurement point. For increasing precision in measurement of the velocity and displacement, it will be necessary to consider the velocity gradient, even in each small region, in the next stage of the research.
2. It is reasonable to consider that each ultrasonic beam passes through the same myocardium for a short period of several tens of ms. However, during one cardiac cycle, it is difficult to track the movement of the myocardium because the direction of the movement does not always coincide with the direction of the ultrasonic beam. To overcome this problem, tracking operation in 2-D or 3-D will be necessary.

In the literature, by transmission of multiple ultrasonic beams, the lateral flow component is determined by correlation using a dual-beam probe (Weiqi and Lin-xin 1982; Overbeck et al. 1992; Routh et al. 1990) or a two-sector transducer probe (Dotti et al. 1992). However, it is not easy to apply these techniques directly to the heart wall, which has complex structure.

In the optical flow technique (Horn and Schunck 1981), cardiac contractility is assessed by decomposing the overall heart wall motion into translation, rotation, deformation and contraction components of the cardiac muscle (Mailloux et al. 1987; Meunier et al. 1989). This method requires extremely long computation time and the decomposed motion components, which are based on the direction of the contrast brightness, are limited to large and slow, which can be recognized in the B-mode image.

In frame-to-frame 2-D correlation analysis of speckle patterns in B-mode images, the lateral and axial components of the 2-D tissue slow motion (Robinson et al. 1982; Trahey et al. 1986; Akiyama et al. 1988; Bohs and Trahey 1991; Chen et al. 1992) or blood flow (Bohs and Trahey 1991; Trahey et al. 1988; Ramamurthy and Trahey 1991) have been assessed. Morsy and von Ramm (1999) tracked tissue motion and blood flow in 3-D by a similar correlation technique. The size of the employed correlation window is coarse, on the order of tens of mm. In these methods, the axial resolution is limited by the center frequency and bandwidth of the US. The lateral resolution is limited by the actual beam-width and the spacing interval of the A-scans. For LV-PW, the typical depth, d , is about 120 mm from the chest surface. The finest lateral resolution r at the LV-PW is $d \tan\{(\pi/2)/240\} \cong d(\pi/480) = 785 \mu\text{m}$, when 240 ultrasonic beams are scanned by a sector-type probe in the 90° range. The achievable lateral resolution is still coarse in the measurement of rapid motion with an amplitude of several μm . Moreover, the typical video frame rate in the 2-D imaging system is on the order of 1/30th of a s. Thus, the acquisition rate is limited to at most on the order of 30 Hz, which is too slow to detect the rapid components. Therefore, the measurement of rapid velocity components in 2-D or 3-D is currently still difficult to realize.

3. Though typical timings have been selected on the order of a few ms, and are displayed in Figs. 8a, 9, 10, 12a, 13a and 14, a continuous display of the 2-D distribution of the instantaneous amplitude and phase would be more effective.
4. In the determination of the propagation delay of the discriminative pulsive wave or irregular vibration due to blood flow among different transmural layers of the

myocardium along a beam direction, the delay time is smaller than that obtained among the different directions of the ultrasonic beam in Fig. 13a. It should be possible to determine accurately such small delay time in the frequency domain using high-frequency components up to 100 Hz.

SUMMARY

In this paper, we have modified a conventional ultrasonic diagnostic system to allow 10 scan lines from a sector scanner to be selected arbitrarily for measurement and analysis, so that the velocity signals can be simultaneously measured at multiple points in the IVS and the LV wall for imaging of their spatial distribution.

By applying this method to healthy subjects and patients with AS in this study, we obtained spatial distributions of small vibrations that were superimposed on the B-mode image. From the results at end-diastole, we confirmed that there is mode-2 eigenvibration on the LV wall. For end-systole, the time delay in the propagation of the steep downward pulses from the root of the aortic valve near the base to the apex can be definitely detected. Moreover, for the ejection period of the patients with AS, irregular vibration components, which correspond to the systolic murmur and have large power, were detected. This method offers potential for imaging of the spatial distribution of small vibrations with high-frequency components, which cannot be recognized by conventional B-mode echocardiography, M-mode echocardiography or by TDI. The method developed herein has potential for application to many patients with various kinds of heart diseases in the near future.

Acknowledgements—The authors are grateful to Prof. Emeritus Noriyoshi Chubachi and Prof. Emeritus Motono Tanaka of Tohoku University, Prof. Floyd Dunn of the Bioacoustics Research Laboratory, the University of Illinois, Prof. Kunio Shirato and Hide-ichi Kamada of Tohoku University School of Medicine, and Dr. Hideyuki Honda of Tohoku Bunka Gakuen University, for helpful discussions. The authors also acknowledge the contributions of Shigemitsu Nakaya and Hideyuki Hasegawa of our laboratory for their support of *in vivo* experiments. This work was supported in part by a Grant-in-Aid for Scientific Research from the Ministry of Education, Science and Culture of Japan.

REFERENCES

- Adler RS, Rubin JM, Bland PH, Carson PL. Quantitative tissue motion analysis of digitized M-mode images: Gestational differences in fetal lung. *Ultrasound Med Biol* 1990;16(6):561–569.
- Akiyama I, Nakajima N, Yuta S. Movement analysis using B-mode images. *Acoust Imaging* 1988;17:499–505.
- Bassini M, Gatti E, Longo T, et al. In vivo recording of blood flow velocity profiles and studies in vitro of profile alterations induced by known stenoses. *Tex Heart Inst J* 1982;9(2):185–194.
- Bohs LN, Trahey GE. A novel method for angle independent ultrasonic imaging of blood flow and tissue motion. *IEEE Trans Biomed Eng* 1991;38(3):280–286.
- Bonnefous O, Pesque P. Time domain formulation of pulse-Doppler ultrasound and blood velocity estimation by cross correlation. *Ultrasound Imaging* 1986;8:73–85.

- Catheline S, Thomas J-L, Wu F, Fink MA. Diffraction field of a low frequency vibration in soft tissues using transient elastography. *IEEE Trans UFFC* 1999;46(4):1013–1019.
- Chen EJ, Jenkins WK, O'Brien WD Jr. The accuracy and precision of estimating tissue displacements using ultrasonic images. *IEEE Ultrason Sympos* 1992:1067–1072.
- Constant J. *Bedside cardiology*. 3rd ed. Boston: Little, Brown and Company, 1985.
- de Jong PGM, Arts T, Hoeks APG, Reneman RS. Determination of tissue motion velocity by correlation interpolation of pulsed ultrasonic echo signals. *Ultrason Imaging* 1990;12:84–98.
- Dickinson RJ, Hill CR. Measurement of soft tissue motion using correlation between A-scans. *Ultrasound Med Biol* 1982;8(3):263–271.
- Donovan CL, Armstrong WF, Bach DS. Quantitative Doppler tissue imaging of the left ventricular myocardium: Validation in normal subjects. *Am Heart J* 1995;130(1):100–104.
- Dotti D, Gatti E, Svelto V, Ugge A, Vidali P. Blood flow measurements by ultrasound correlation techniques. *Energia Nucleare* 1976;23(11):571–575.
- Dotti D, Lombardi R, Piazzi P. Vectorial measurement of blood velocity by means of ultrasound. *Med Biol Eng Comput* 1992;30:219–225.
- Fleming AD, Xia X, McDicken WN, Sutherland GR, Fenn L. Myocardial velocity gradients detected by Doppler imaging. *Br J Radiol* 1994;67:679–688.
- Forbes CD, Jackson WF. *Color atlas and text of clinical medicine*. 2nd ed. London: Mosby-Wolfe, 1997:239.
- Goecsan J III, Gulati VK, Mandarino WA, Katz WE. Color-coded measures of myocardial velocity throughout the cardiac cycle by tissue Doppler imaging to quantify regional left ventricular function. *Am Heart J* 1996;131:1203–1213.
- Groves DH, Powlowski T, White DN. A digital technique for tracking moving interfaces. *Ultrasound Med Biol* 1982;8(2):185–190.
- Hartley CJ, Litowitz H, Rabinovitz RS, et al. An ultrasonic method for measuring tissue displacement: Technical details and validation for measuring myocardial thickening. *IEEE Trans Biomed Eng* 1991;38(8):735–747.
- Heimdahl A, Støylen A, Drtecht HT, Skjærpe T. Real-time Strain rate imaging of the left ventricle by ultrasound. *J Am Soc Echocardiogr* 1998;11:1013–1019.
- Hein IA, O'Brien WD Jr. A real-time ultrasound time-domain correlation blood flowmeter: Part II—Performance and experimental verification. *IEEE Trans UFFC* 1993;40(6):776–785.
- Hein IA, Chen JT, Jenkins WK, O'Brien WD Jr. A real-time ultrasound time-domain correlation blood flowmeter: Part I—theory and design. *IEEE Trans UFFC* 1993;40(6):768–775.
- Hein IA, Novakofski J, Nostwick L, O'Brien WD Jr. Application of ultrasound time-domain correlation to the aging of porcine muscle for the first twenty-four hours post mortem. *Acoust Imaging* 1992;19:403–407.
- Hoeks APG, Brands PJ, Smeets FAM, Reneman RS. Assessment of the distensibility of superficial arteries. *Ultrasound Med Biol* 1990;16(2):121–128.
- Hokanson DE, Monzersky DJ, Sumner SD, Strandness DE Jr. A phase-locked echo tracking system for recording arterial diameter changes in vivo. *J Appl Physiol* 1972;32(5):728–733.
- Hokanson DE, Strandness DE Jr, Miller CW. An echo-tracking system for recording arterial wall motion. *IEEE Trans Sonic Ultrason* 1970;SU-17(3):130–132.
- Honda H, Koiwa Y, Takagi K, et al. Noninvasive measurement of left ventricular myocardial elasticity. *Am J Physiol* 1994;266(35):H881–H890.
- Honda H, Nakaya S, Kamada H, et al. Non-invasive estimation of human left ventricular end-diastolic pressure. *Med Eng Phys* 1998;20:485–488.
- Horn BKP, Schunck BG. Determining optical flow. *Artificial Intelligence* 1981;17:185–203.
- Janssen PML, Honda H, Koiwa Y, Shirato K. The effect of diastolic vibration on the relaxation of rat papillary muscle. *Cardiovasc Res* 1996;32:344–350.
- Jensen JA. Detection probabilities for time-domain velocity estimation. *IEEE Ultrason Sympos* 1991:1291–1296.
- Kanai H, Hasegawa H, Chubachi N, Koiwa Y, Tanaka M. Noninvasive evaluation of local myocardial thickening and its color-coded imaging. *IEEE Trans UFFC* 1997;44(4):752–768.
- Kanai H, Koiwa Y, Zhang J. Real-time measurements of local myocardium motion and arterial wall thickening. *IEEE Trans UFFC* 1999a;46(5):1229–1241.
- Kanai H, Nakaya S, Honda H, Koiwa Y. Noninvasive estimation of left-ventricular end-diastole elasticity by analyzing heart wall vibrations. *Electron Lett* 1999b;35(10):765–766.
- Kanai H, Sato M, Koiwa Y, Chubachi N. Transcutaneous measurement and spectrum analysis of heart wall vibrations. *IEEE Trans UFFC* 1996;43:791–810.
- Kanai H, Sugimura K, Koiwa Y, Tsukahara Y. Accuracy evaluation in ultrasonic-based measurement of microscopic change in thickness. *Electron Lett* 1999c;35(12):949–950.
- Korba LW, Cobbold RSC, Cousin AJ. An ultrasonic imaging and differential measurement system for the study of fetal respiratory movements. *Ultrasound Med Biol* 1979;5:139–148.
- Koiwa Y, Honda H, Takagi T, et al. Modification of human left ventricular relaxation by small-amplitude phase-controlled mechanical vibration on the chest wall. *Circulation* 1997;95(1):156–162.
- Koiwa Y, Ohyama T, Takagi T, et al. The left ventricular vibration mode in the ventricular transfer function method and at the moment of the first heart sound. *Front Med Biol Eng* 1988;1(1):59–70.
- Lerner RM, Huang SR, Parker KJ. Sonoelasticity images derived from ultrasound signals in mechanically vibrated tissues. *Ultrasound Med Biol* 1990;16(3):231–239.
- Mailloux GE, Bleau A, Bertrand M, Petitclerc R. Computer analysis of heart motion from two-dimensional echocardiograms. *IEEE Trans Biomed Eng* 1987;BME-34(5):356–364.
- Meunier J, Bertrand M, Mailloux GE, Petitclerc R. Local myocardial deformation computed from speckle motion. *IEEE Comput Cardiol* 1989:133–136.
- Mirsky I, Ghista DN, Sandler H. *Cardiac mechanics: Physiological, clinical, and mathematical considerations*. New York: Wiley & Sons, 1974:331–358.
- Miyatake K, Yamagishi M, Tanaka N, et al. New method for evaluating left ventricular wall motion by color-coded tissue Doppler imaging: In vitro and in vivo studies. *J Am Coll Cardiol* 1995;25:717–724.
- Morsy AA, von Ramm OT. FLASH correlation: A new method for 3-D ultrasound tissue motion tracking and blood velocity estimation. *IEEE Trans UFFC* 1999;46(3):728–736.
- Ophir J, Céspedes I, Ponnekanti H, Yazdi Y, Li X. Elastography: A quantitative method for imaging the elasticity of biological tissues. *Ultrason Imaging* 1991;13:111–134.
- Overbeck JR, Beach KW, Strandness DE Jr. Vector Doppler: Accurate measurement of blood velocity in two dimensions. *Ultrasound Med Biol* 1992;18(1):19–31.
- Palka P, Lange A, Fleming AD, et al. Doppler tissue imaging: Myocardial wall motion velocities in normal subjects. *J Am Soc Echocardiogr* 1995;8(5 part 1):659–668.
- Palka P, Lange A, Fleming AD, et al. Age-related transmural peak mean velocities and peak velocity gradients by Doppler myocardial imaging in normal subjects. *Eur Heart J* 1996;17:940–950.
- Parker KJ, Huang SR, Musulin RA, Lerner RM. Tissue response to mechanical vibrations for sonoelasticity imaging. *Ultrasound Med Biol* 1990;16(3):241–246.
- Powlowski T. Ultrasonic system for noninvasive measurement of hemodynamic parameters of human atrial vascular system. *Arch Acoustics* 1988;13(1–2):89–108.
- Ramamurthy BS, Trahey GE. Potential and limitations of angle-independent flow detection algorithms using radio-frequency and detected echo signals. *Ultrason Imaging* 1991;13:252–268.
- Rapoport I, Cousin AJ. New phase-lock tracking instrument for foetal breathing monitoring. *Med Biol Eng Comput* 1982;20:1–6.
- Robinson DE, Chen F, Wilson LS. Measurement of velocity of propagation from ultrasonic pulse-echo data. *Ultrasound Med Biol* 1982;8(4):413–420.

- Routh HF, Pusateri TL, Waters DD. Preliminary studies into high velocity transverse blood flow measurement. *IEEE Ultrasonics Sympos* 1990;1523–1526.
- Sainz A, Roberts VC, Pinardi G. Phased-locked loop techniques applied to ultrasonic Doppler signal processing. *Ultrasonics* 1976;14:128–133.
- Sato M, Kanai H, Chubachi N, Honda H, Koiwa Y. Method for noninvasive estimation of left ventricular end diastolic pressure based on analysis of heart wall vibration. *Electron Lett* 1996;32(11):949–950.
- Suorsa V, Kerr AT, Hunt JW, O'Brien WD Jr. Influence of stationary signals on the time-domain correlation blood flow measurement. *IEEE Ultrason Sympos* 1990:1563–1566.
- Sutherland GR, Stewart MJ, Groundstroem KWE, et al. Color Doppler myocardial imaging: A new technique for the assessment of myocardial function. *J Am Soc Echocardiog* 1994;7:441–458.
- Trahey GE, Hubbard SM, von Ramm OT. Angle independent ultrasonic blood flow detection by frame-to-frame correlation of B-mode images. *Ultrasonics* 1988;26:271–276.
- Trahey GE, Smith SW, von Ramm OT. Speckle pattern correlation with lateral aperture translation: Experimental results and implications for spatial compounding. *IEEE Trans UFFC* 1986;UFFC-33(3):257–264.
- Tristram M, Barbosa DC, Cosgrove DO, Bamber JC, Hill CR. Application of Fourier analysis to clinical study of patterns of tissue movement. *Ultrasound Med Biol* 1988;14(8):695–707.
- Uematsu M, Miyatake K, Tanaka N, et al. Myocardial velocity gradient as a new indicator of regional left ventricular contraction: Detection by a two-dimensional tissue Doppler imaging technique. *J Am Coll Cardiol* 1995;26(1):217–223.
- Watanabe F, Takenaka K, Sonoda M, et al. Validation of a new method of obtaining purely regional LV wall motion velocity color maps: In vitro and in vivo studies. *Circulation* 1997;96(Suppl. I):I-714.
- Wei-qi W, Lin-xin Y. A double beam Doppler ultrasound method for quantitative blood flow velocity measurement. *Ultrasound Med Biol* 1982;8(4):421–425.
- Yamakoshi Y, Sato J, Sato T. Ultrasonic imaging of internal vibration of soft tissue under forced vibration. *IEEE Trans UFFC* 1990;37:45–53.
- Yamazaki N, Mine Y, Sano A, et al. Analysis of ventricular wall motion using color-coded tissue Doppler imaging system. *Jpn J Appl Phys* 1996;33(5B):3141–3146.